energies

MDPI

Article

Confronting Land Surface Temperature and Ground Station Data for Urban Heat Island Assessment and Urban Building Energy Modeling—A Case Study for Northern Italy

Mario Alves da Silva *, Gregorio Borelli, Andrea Gasparella and Giovanni Pernigotto *

Faculty of Engineering, Free University of Bozen-Bolzano, 39100 Bolzano, Italy;
gregorio.borelli@student.unibz.it (G.B.); andrea.gasparella@unibz.it (A.G.)
* Correspondence: mario.alvesdasilva@unibz.it (M.A.d.S.); giovanni.pernigotto@unibz.it (G.P.)

Abstract

Data scarcity limits robust assessment of urban overheating and its implications for building energy use, especially in complex-terrain cities such as those in mountain environments. In this context, Land Surface Temperature (*LST*) from thermal remote sensing can be used to map urban hotspots at high spatial resolution. Nevertheless, it does not provide the full set of hourly atmospheric variables required to run building energy simulations aimed at quantifying their impact and defining mitigation measures. Given these premises, this study proposes a methodology combining satellite-derived *LST* with ground meteorological measurements to assess Urban Heat Island (*UHI*) patterns and quantify how measured weather data selection affects urban building energy modeling (*UBEM*) outcomes. After selecting as a case study Bolzano, an Alpine city in Northern Italy, ECOSTRESS *LST* (2019–2025, May–August) was first processed and quality-screened to (1) compute Δ*LST* (urban–rural) and (2) identify diurnal and spatial overheating patterns across the building stock. Second, four measured weather datasets—one rural station and three urban stations located in the city core, in the industrial district, and in the urban edge—were used as boundary conditions in an EnergyPlus-based *UBEM* parametric campaign for 253 residential buildings, covering multiple envelope insulation levels and window-to-wall ratios. Results show strong diurnal asymmetry in surface overheating, with the largest contrasts in the afternoon and prominent industrial hotspots. Ground measurements confirm persistent intra-urban microclimatic differences, and the choice of measured weather dataset causes systematic shifts in simulated cooling demand and thermal comfort. The study highlights the need for weather data selection strategies based on microclimatic context rather than simple proximity, improving representativeness in *UBEM* applications for Alpine and other heterogeneous urban environments.

Keywords: urban heat island; land surface temperature; ECOSTRESS; ground meteorological stations; weather data representativeness; urban building energy modeling; cooling demand; thermal comfort

Check for updates

Academic Editor: Paulo Santos

Received: 24 December 2025
Revised: 22 January 2026
Accepted: 26 January 2026
Published: 29 January 2026

Copyright: © 2026 by the authors. Licensee MDPI, Basel, Switzerland. This article is an open access article distributed under the terms and conditions of the Creative Commons Attribution (CC BY) license.

1. Introduction

Urban areas sit at the center of Europe's climate and energy transition. They concentrate population, infrastructure, and energy use. They are also characterized by high overheating risk due to heat waves and local microclimatic phenomena. Recent European assessments show that progress in the building sector is still not fast enough to meet 2030

 https://doi.org/10.3390/en19030724

and 2050 targets [1]. In this scenario, Alpine and mountain regions add another layer of complexity. Projections for the European Alps indicate strong warming and relevant changes in extremes [2]. For Northern Italy, this matters because many cities lie in valleys or near mountain foothills. In these settings, local climate, urban form, and energy demand are tightly coupled [3,4].

A key driver of urban overheating is the Urban Heat Island (*UHI*) effect. Urban areas often remain warmer than nearby rural areas. This is linked to heat storage in materials, reduced evapotranspiration, and altered radiation and airflow. The Local Climate Zone (*LCZ*) framework provides a standard way to describe these urban–rural contrasts across cities and neighborhoods [5]. Mediterranean and Italian studies show that *UHI* intensity depends strongly on urban texture. Density, vegetation, and surface properties are recurrent factors [6]. *UHI* also changes in time. Seasonal and diurnal variability can be large, and it affects both surface and near-surface conditions [7]. Reviews across climates confirm that *UHI* and its counterpart phenomena can differ by context, reinforcing the need for location-specific assessment [8].

Land Surface Temperature (*LST*) from thermal infrared remote sensing is widely used to map where cities overheat. It offers spatial detail that dense ground networks rarely provide. *LST* also supports analysis of land-cover drivers of heat. Complementary satellite products, such as Sentinel-2-derived vegetation indices (e.g., the Normalized Difference Vegetation Index, *NDVI*) and land-cover datasets, are often used alongside *LST* to characterize surface properties, vegetation patterns, and urban structure that modulate surface heating, as shown in *LST–LULC* (Land Use and Land Cover) and *NDVI*-based *UHI* studies [9–12]. Studies have used *LST* to relate surface temperature to urban expansion, imperviousness, and vegetation patterns [9,10]. Similar approaches have been applied in different contexts to quantify how land-cover change modifies thermal patterns [11]. These strengths make *LST* useful in identifying hotspots and spatial gradients within a city. Recent sensors improve this picture further. ECOSTRESS, for instance, provides high spatial resolution and samples at different times of day. This enables analysis of diurnal surface heat dynamics and intra-urban contrasts [13]. *LCZ*-based studies that combine ECOSTRESS with other satellites show systematic differences between compact, open, and vegetated urban classes [14]. Combining ECOSTRESS with Landsat has also strengthened the interpretation of patterns in Mediterranean settings [15]. Italian case studies highlight that, even within the same *LCZ*, *LST* can vary markedly across neighborhoods and between cities [16].

However, *LST* is not the same variable used in most building energy simulations. *LST* represents surface "skin" temperature, not the air temperature that drives convective heat exchange at façade and roof level. The relationship between *LST* and air temperature depends on land cover, atmospheric conditions, and time of day [12]. Remote sensing retrievals also carry their own uncertainties. Urban *LST* can vary with view angle and 3D geometry, which affects the radiance sampled by a sensor [17]. Broader reviews of remote-sensing data quality stress that careful processing and interpretation are needed, especially in urban applications [18]. These limitations do not reduce the value of *LST* for mapping patterns. On the contrary, they do highlight that *LST* alone is not sufficient when the aim is to drive building energy modeling.

Building energy performance is highly sensitive to weather boundary conditions. This is especially true for cooling demand. Research on urban microclimates and building performance shows that local conditions can shift predicted loads, sometimes substantially [19]. Studies that frame microclimate as a boundary condition problem stress that urban-scale deviations from standard meteorological data can alter simulation outcomes [20]. Reviews linking *UHI* and energy confirm that urban warming increases cooling demand and that

the effect can be non-negligible in dense settings [21]. Urban morphology adds further structure. In dense fabrics, shading, sky-view factor, and ventilation constraints can modify both exposure and heat dissipation [22].

These issues become sharper at district scale. Urban Building Energy Modeling (*UBEM*) extends building simulation to many buildings and neighborhoods. Reviews of *UBEM* identify microclimate inputs as a key source of uncertainty, because they affect all buildings simultaneously [23]. Broader reviews of urban microclimates and energy modeling make the same point. They stress that climate–energy coupling is often limited by the quality and representativeness of local weather data [24]. The "ten questions" perspective on *UBEM* explicitly places local weather representation among the central technical challenges [25].

Several tools try to fill the gap between rural weather files and urban conditions. The Urban Weather Generator (*UWG*) is one of the most used. It morphs rural weather into an urban series using simplified canopy physics and morphology parameters. Recent reviews discuss its development, applications, and current limitations [26]. Work on weather data for building simulation also emphasizes that uncertainty in weather inputs can propagate strongly into energy results, especially when modeling cooling and extremes [27]. For Mediterranean contexts, empirical and parametric studies show that morphology and anthropogenic heat assumptions can influence simulated *UHI* intensity, which in turn affects building loads [28]. These studies also imply a practical point: modeled urban weather is only as good as its inputs and its validation.

This is where ground measurements become particularly valuable. Weather stations directly measure air temperature, humidity, wind speed, and radiation at high temporal resolution. These variables match what energy models need. They also provide an anchor for validating or correcting modeled microclimates. Several studies that couple microclimate and building performance underline the importance of measured conditions and the implications of station representativeness [6,19]. Morphological variability also matters for representativeness. Cities contain many distinct block types and local climates, even within the same broad class [29]. Italian evidence during heatwaves further shows that the same region can host very different thermal responses, tied to morphology and land cover [30]. Taken together, this supports a practical strategy: use *LST* to locate and characterize hotspots, then use ground stations to provide the time-resolved atmospheric boundary conditions that energy models require.

Most studies still treat *UHI* mapping and building-energy boundary conditions as separate steps. Remote sensing is used to locate hotspots, while energy simulations often rely on a single reference weather file or on whichever station data are easiest to access. The spatial structure revealed by *LST* is therefore not always used to guide the selection of representative ground measurements for specific neighborhoods. This disconnect is frequently highlighted in *UBEM* discussions, where local weather representativeness is repeatedly cited as a key source of uncertainty [23,25].

Research Significance

This work addresses a recurrent limitation in urban-scale energy assessments: *UHI* mapping and the definition of weather boundary conditions for building simulations are often treated as separate steps, which can lead to non-representative microclimatic inputs in *UBEM* workflows. Therefore, this study proposes an integrated approach that combines satellite-derived land surface temperature (*LST*) with ground meteorological observations. *LST* is used to delineate *UHI*-prone areas and intra-urban thermal gradients, while ground stations provide the hourly atmospheric boundary conditions required by building energy models and support the evaluation of station representativeness across

different urban contexts. Finally, the study quantifies how the selection of measured weather datasets propagates into simulated space-cooling energy demand and indoor thermal comfort outcomes.

The novelty lies in (i) using multi-temporal *LST* patterns to inform the interpretation of intra-urban microclimates, and (ii) testing multiple urban station types (urban core, industrial district, and urban–rural edge) rather than relying on a single "urban" dataset, which is still common practice. In addition, representativeness is evaluated beyond spatial proximity by explicitly assessing how weather station choice affects simulation outputs across a large parametric building set, and by testing whether distance is a reliable proxy for weather assignment.

2. Methods

This section presents an integrated workflow that links satellite-derived surface thermal patterns with ground meteorological measurements to assess *UHI* intensity and its implications for *UBEM*. First, ECOSTRESS land surface temperature (*LST*) scenes are screened and processed to map urban–rural thermal contrasts across diurnal periods and years. Second, measurements from multiple urban stations and one rural reference station are quality-checked, harmonized to an hourly timestep, and formatted as EnergyPlus Weather (EPW) files. Finally, these station-specific weather files are used as boundary conditions in a parametric *UBEM* campaign to quantify how microclimatic forcing affects cooling needs and comfort, and to evaluate station representativeness (Figure 1).

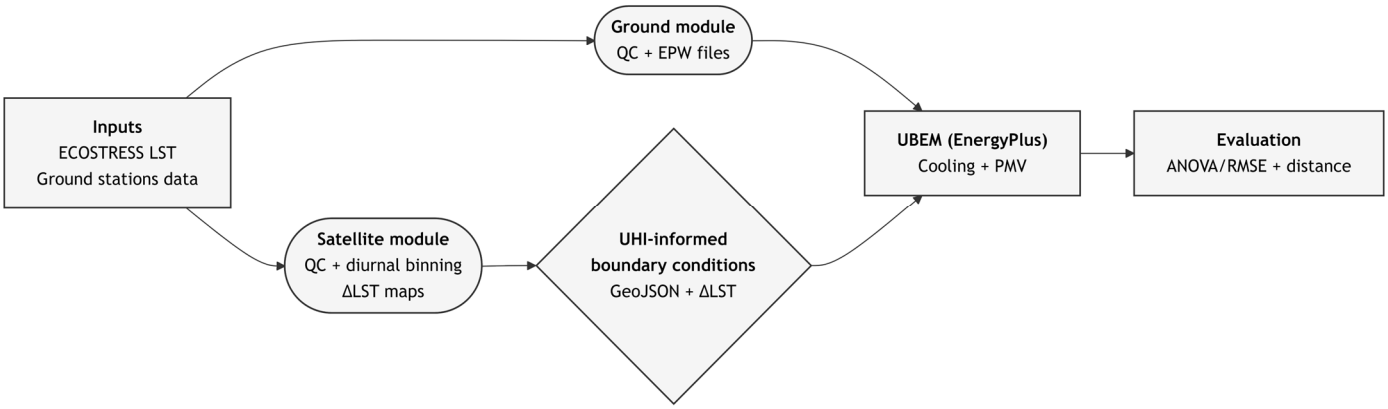

Figure 1. Workflow of the proposed methodology, integrating satellite-derived land surface temperature (*LST*) and ground station measurements and performing a quality check (*QC*) to characterize Urban Heat Island (*UHI*) patterns and Urban Building Energy Modeling (*UBEM*) in terms of both space cooling need and indoor Predicted Mean Vote (*PMV*).

2.1. Location Definition

This study focused on the city of Bolzano, located in the northern part of Italy, between different climate borders. According to the Koppen-Geiger classification, Bolzano has a humid subtropical climate (*Cfa*), with hot summers and cold winters. From a building energy perspective, based on the Italian heating degree-day (*HDD*) classification, Bolzano is located within Climate Zone E, i.e., with *HDD* with respect to a 20 °C base temperature ranging from 2101 K d to 3000 K d, with a historically dominant building design focusing on heating needs. However, climate change led to a significant increase in the air temperature and, consequently, higher space cooling needs. The Statistical Office of the European Union (*Eurostat*) shows Bolzano with 222 K d cooling degree days (*CDD*) according to a base temperature of 21 °C [31], indicating significant cooling energy needs. Data retrieved from the Italian Institute for Environmental Protection and Research—*ISPRA* [32]—show the variation in the climate normals for Bolzano from 1961 to 2020 (Figure 2). In particular,

these data highlight that, from May to August, there is a consistent increase in the air temperature records. The mean air temperature and the maximum air temperature clearly display a positive trend based on 60 years of data.

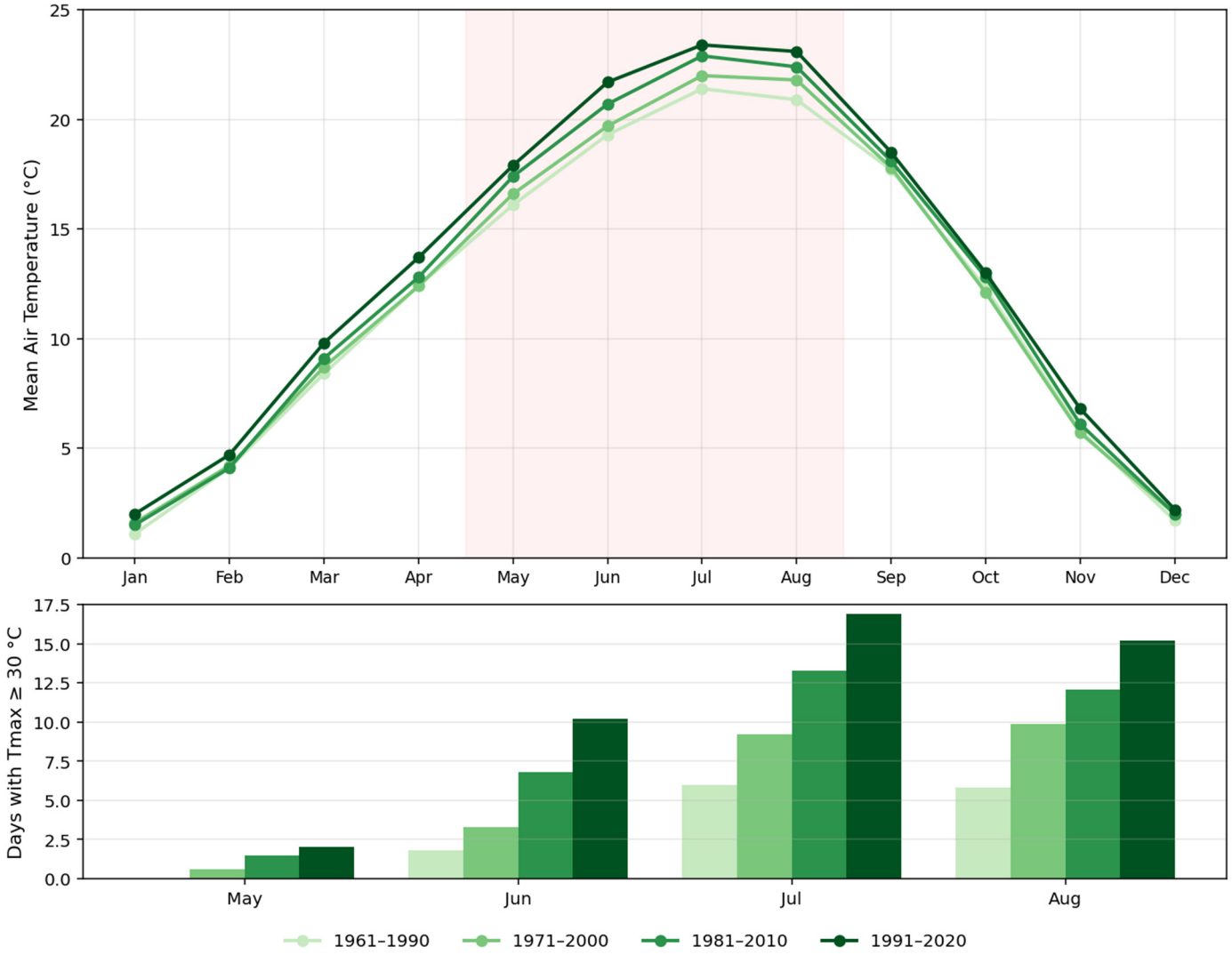

Figure 2. Mean monthly air temperature in Bolzano for four official ISPRA climate-normal periods (1961–1990, 1971–2000, 1981–2010, 1991–2020) is shown in the (**top panel**), with the red-shaded region marking the months considered in this study. The (**bottom panel**) reports the number of days with maximum air temperature ≥30 °C for the months of interest.

Throughout the year, all months showed a significant temperature increase, with May to August displaying a temperature variation above 1.5 °C. The severity of the temperature variation is even more marked from June to August, where the temperature showed an increase above 2 °C. Therefore, this preliminary assessment led to the definition of the period between May and August as the timeframe of this study.

2.2. Satellite Data Processing and UHI Characterization

Weather data were first retrieved from the ECOSTRESS database with a native resolution of 70 m and used for a Land Surface Temperature (*LST*) analysis [33], considering all available records from 2019 to 2025, from May to August.

Since the *UHI* mainly describes the temperature increase in the urban areas in respect to the rural regions, we determined the urban boundaries (Figure 3a) and the corresponding rural environment (Figure 3b). The urban polygon corresponds to the limits of the urban

settlement of Bolzano and tries to encompass most of the buildings within the city. We defined the rural area based on its climatic and topographical similarities with Bolzano, even though the perimeter is within a neighboring city and 7 km far from the defined urban boundaries (Figure 3c). Furthermore, the rural polygon was set as a circular buffer with a 100 m radius, using an existing ground station as its center. The 100 m buffer was selected to maintain homogeneous land-cover conditions around the reference station and to reduce mixed-pixel effects at the ECOSTRESS spatial resolution. The 7 km distance reflects the local valley morphology and station availability, providing a comparable topographic setting, while remaining outside the continuous built-up area.

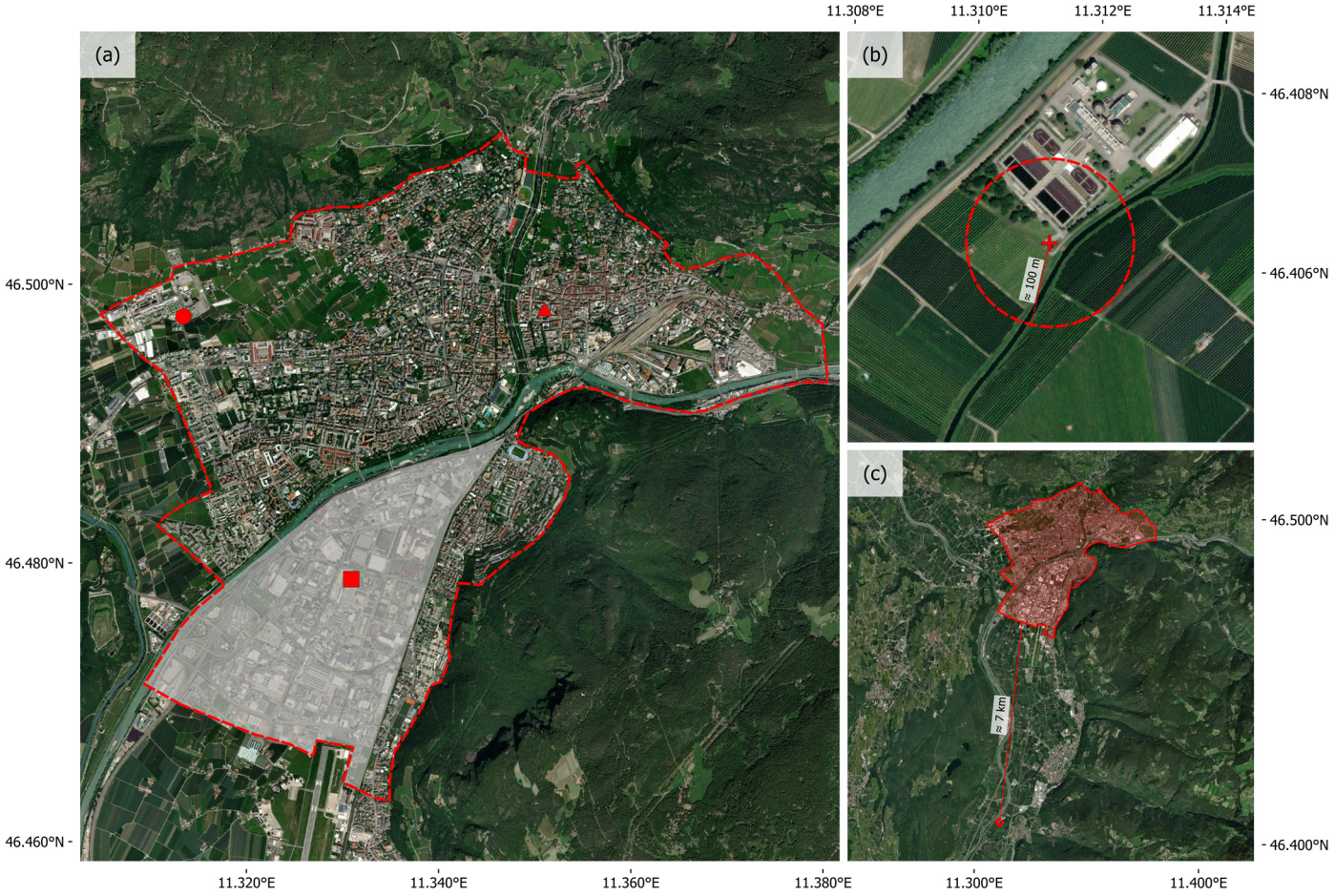

Figure 3. Urban delimitation of Bolzano with the weather stations *SU1* (red triangle), *SU2* (red square), and *SU3* (red circle), and the delimitation of the industrial zone, highlighted in grey (**a**). Rural polygon and the rural weather station *SR* (red cross) (**b**). Distance between the boundaries defined for the urban and rural regions (**c**).

Following the downloading of the satellite data, the raw content was processed to keep only images with the correct geographical reference, low cloud cover, and reasonable temperature limits within the pixels. For each image, rural and urban, the average of all pixels should be greater than 0, since we are dealing with a summer period. Additionally, we set a deviation threshold of 30 °C, e.g., the image was discarded in case the difference between maximum and minimum pixel values was greater than 30 °C. The quality control process was carried out for each image, considering the urban and rural areas independently. For each good-quality image, we computed the urban–rural surface temperature contrast at pixel level as: $\Delta LST = LST_{urban,pixel} - LST_{rural,mean}$, where $LST_{urban,pixel}$ is the *LST* for each pixel within the urban area and $LST_{rural,mean}$ is the mean *LST* within the rural reference polygon for

the same image. With this definition, positive Δ*LST* values indicate a warmer urban surface relative to the rural reference. After calculating the difference for all images, they were grouped to assess the *UHI* effect by year and period of the day, considering four different ranges: 12 a.m.–6 a.m., 6 a.m.–1 p.m., 1 p.m.–8 p.m., and 8 p.m.–12 a.m. Then, for each year and period of the day, all good quality images were averaged to assess the *UHI* effect.

After calculating the Δ*LST* for the urban area of Bolzano, we used a CityJSON file containing all the buildings of Bolzano to determine the Δ*LST* of each one of them (Figure 4). The use of CityJSON files in *UBEM* studies is reported in many cases [34,35], since the file contains the 3D information required for the simulation. In our study, the CityJSON file was created using GIS data provided by the Municipality of Bozen-Bolzano and buildings' heights were determined according to Digital Surface Model (*DSM*) and Digital Terrain Model (*DTM*) records from the Autonomous Province of Bolzano/Bozen—South Tyrol [36]. The CityJSON also grouped the buildings in four groups: residential, commercial, industrial, and others. Therefore, the *UHI* effect was identified for each construction throughout the years and period of the day, allowing the identification of critical areas and buildings.



Figure 4. Spatial distribution of buildings within the urban area of Bolzano, classified by end use. Residential buildings are shown in blue, commercial buildings in yellow, industrial buildings in grey, and other end uses in brown. The central panel presents the complete urban footprint within the municipal boundary (dashed red line), together with the locations of weather stations *SU1* (red triangle), *SU2* (red square), and *SU3* (red circle). The surrounding panels display selected local 3D views of representative city sub-areas, where building footprints are extruded according to average building height and colored consistently with the end-use classification shown in the central map.

2.3. Ground Stations' Data Retrieval and Processing

In the context of *UHI* and Urban Building Energy Modeling, most studies focus on the adaptation of rural weather files to the microclimate context to obtain more reliable energy needs estimations. In this study, we investigated a different approach, based on the application of weather data measurements within the city to properly characterize the local microclimate. Within the urban boundaries of Bolzano, this study considered three meteorological stations (Figure 3a), located in the city center (*SU1*), industrial zone (*SU2*), and the final one located at the boundary with the rural and mountainous environment (*SU3*). The station within the rural polygon was named "*SR*". Regarding the morphological aspects, *SU1* is located within the urban core but placed over a green roof with more than 700 m^2 and less than 200 m distant from a river and a park. *SU2* sits within a typical industrial area, with a high occurrence of impervious surfaces. The last urban station, *SU3*, is located at the boundaries of a lower-density urban area and the rural and mountainous environment.

To provide a standardized description of station surroundings, we additionally characterized each site using the Local Climate Zone (*LCZ*) framework and the global *LCZ* map provided by the *LCZ Generator* [37]. The rural station *SR* is located in a transition landscape, with an *LCZ* at the station point corresponding to open low-rise (*LCZ 6*) and a mixed surrounding composition dominated by sparsely built (*LCZ 9*) and dense trees (*LCZ A*) within 250–1000 m. The urban-core station *SU1* is classified as compact midrise (*LCZ 2*) at the point location, but its surroundings become increasingly heterogeneous, shifting toward open midrise (*LCZ 5*) as the dominant class at 500–1000 m. This mixed *LCZ* context is consistent with the presence of nearby non-built surfaces within the central urban area and supports the interpretation of *SU1* as a locally moderated urban site. The industrial-district station *SU2* is mapped as large low-rise (*LCZ 8*) and shows the most homogeneous surroundings, with *LCZ 8* dominating at 250–500 m. The urban–rural edge station *SU3* is also classified as large low-rise (*LCZ 8*) at the point location, but it lies closer to *LCZ* transitions and exhibits a mixed buffer composition, with increasing shares of natural classes (e.g., scattered trees, *LCZ B*) and low-rise/open forms at larger radii. Overall, the *LCZ* analysis confirms that the four stations represent distinct microclimatic contexts and provide a transferable basis for discussing station representativeness beyond proximity alone.

SU3 and *SR* belong to the network of the Autonomous Province of Bolzano/Bozen—South Tyrol and have 10 min records of air temperature, relative humidity, solar radiation, wind speed and wind direction. *SU1* and *SU2* belong to the Free University of Bozen-Bolzano and measure data with a 1 min resolution. *SU1* provides air temperature, relative humidity, global horizontal radiation, diffuse horizontal radiation, and direct normal radiation, but it does not measure wind speed or direction. *SU2* provides air temperature, relative humidity, global horizontal radiation, diffuse horizontal radiation, and wind speed and direction. For subsequent use in the *UBEM* simulations, the weather data were compiled according to the EPW format (EnergyPlus Weather File). Despite the *UHI* analysis considering ECOSTRESS records from May to August (2019–2025), the ground-based comparison and the *UBEM* simulations were limited to June–August 2021 due to data availability and to ensure a continuous period with minimal gaps. This timeframe is therefore intended as a preliminary summer validation and sensitivity test, and it does not capture the full seasonal variability of urban thermal behavior. Consequently, the interpretation focuses on warm-season conditions and avoids generalizing station representativeness to the annual scale.

2.4. Urban Building Energy Modeling Settings and Simulation

The energy simulations focused on a subset of the residential building stock within the urban perimeter of Bolzano (253 buildings, corresponding to 5% of the stock), selected to represent both morphological variability and *UHI* exposure. Selection criteria included building height, volume, spatial distribution across the city, and shading angle from surrounding obstructions, together with the *LST*-derived *UHI* intensity. Specifically, buildings were ranked using ΔLST during the warmest diurnal window in 2021, and the final subset was assembled to include constructions spanning low to high ΔLST conditions rather than clustering only on hotspots. The *UBEM* process was carried out in EnergyPlus 23.2, with each building simulated at a time and the surrounding being considered as shading elements to reduce the computational burden of the process. No moveable shading devices were added to the building in order to get the extreme effects related to heat gains from solar radiation. Considering the availability of the weather files, as shown in Section 2.3, the simulation was run from June to August for all four weather stations.

The simulation process considered three construction settings for the building envelope: non-insulated, well-insulated, and nearly-zero energy buildings (*nZEB*), reported in Table 1. The non-insulated configuration adopted clay brick material for the envelope and a double-pane window. The well-insulated envelope added an insulation layer to the clay brick material and changed the windows to a triple-glazing system. For the *nZEB* models, the opaque envelope had the same construction as the insulated building, but the triple-glazing system was replaced with a triple-glazing low-e system. Additionally, the parametric simulation also considered a variation from 10% to 90% on the window-to-wall ratio (*WWR*), with steps of 10 percentage points.

Table 1. *U*-value for the envelope surfaces and windows according to the different building construction settings.

Building Envelope Surface	Non-Insulated	Well-Insulated	*nZEB*
Opaque	1.05 W m^{-2} K^{-1}	0.19 W m^{-2} K^{-1}	0.19 W m^{-2} K^{-1}
Window	3.12 W m^{-2} K^{-1}	1.62 W m^{-2} K^{-1}	1.06 W m^{-2} K^{-1}

Fixed convective coefficients were adopted during the simulation process. The opaque exterior surfaces had a coefficient of 24.67 W m^{-2} K^{-1}, the windows had a coefficient of 16.37 W m^{-2} K^{-1}, and the interior surfaces had a coefficient of 3.16 W m^{-2} K^{-1} [38]. Internal gains for occupancy, lighting, and appliances were defined according to EN 16798-1 [39] and EN 15193-1 [40]. The infiltration and ventilation rate varied according to each thermal zone height to attend also to the minimum hygienic ventilation rate of 0.5 l/(s·m^2), as specified on EN 16798-1 [39], which also satisfies the requirements of local laws of 0.5 ACH [41]. For the conditioning strategy, we adopted an ideal load system to address the cooling needs with a 26 °C setpoint available during the entire occupied period.

We requested the hourly cooling energy to analyze the Ideal Loads system, while the hourly Predicted Mean Vote (*PMV*) [39,42] were used to assess the occupants' thermal comfort based on a clothing insulation of 0.5 clo and a metabolic rate of approximately 1.14 met, based on the occupancy density of 28.3 m^2/person and internal loads of 4.2 W/m^2, as specified on EN 16798-1 [39].

2.5. Representativeness and Sensitivity Metrics

The simulation outputs were used to compare the rural and urban weather files, and the impact of the different urban weather stations in the simulation results. An ANOVA test based on mixed-effects model was used to determine the statistical significance of the different weather files, building envelope materials and *WWR*, on the total energy

needs, and the average *PMV*. The ANOVA model fit was quantified with the marginal R^2 (fixed effects) and conditional R^2 (fixed + random effects), following Nakagawa and Schielzeth [43], while the factor effect size was measured by the η^2. The effect sizes were classified according to Richardson [44]: negligible (<0.01), small (0.01–0.06), medium (0.06–0.14), and large ($\geq$0.14).

To quantify deviations between weather stations, *RMSE* was computed using hourly values and then aggregated at sub-daily and daily time scales through pairwise comparisons among the four weather files. Finally, to test whether spatial proximity explains representativeness, building–station distance was compared against *RMSE* using both Pearson's correlation coefficient (linear association) and Spearman's rank correlation coefficient (monotonic association). This analysis was used to evaluate whether distance provides a reliable criterion for selecting urban weather stations in *UBEM* simulations.

3. Results and Discussion

3.1. Urban Heat Island Assessment: LST and Air Temperature

The raw sample of satellite data contained 229 images that went through quality control and resulted in a sample of 119 images identifying the variation between the *LST* in the urban and the rural perimeters (Figure 5). Across the different years, the results show a clear and consistent diurnal asymmetry between the established daily intervals, but a consistent pattern for the different periods across the years.

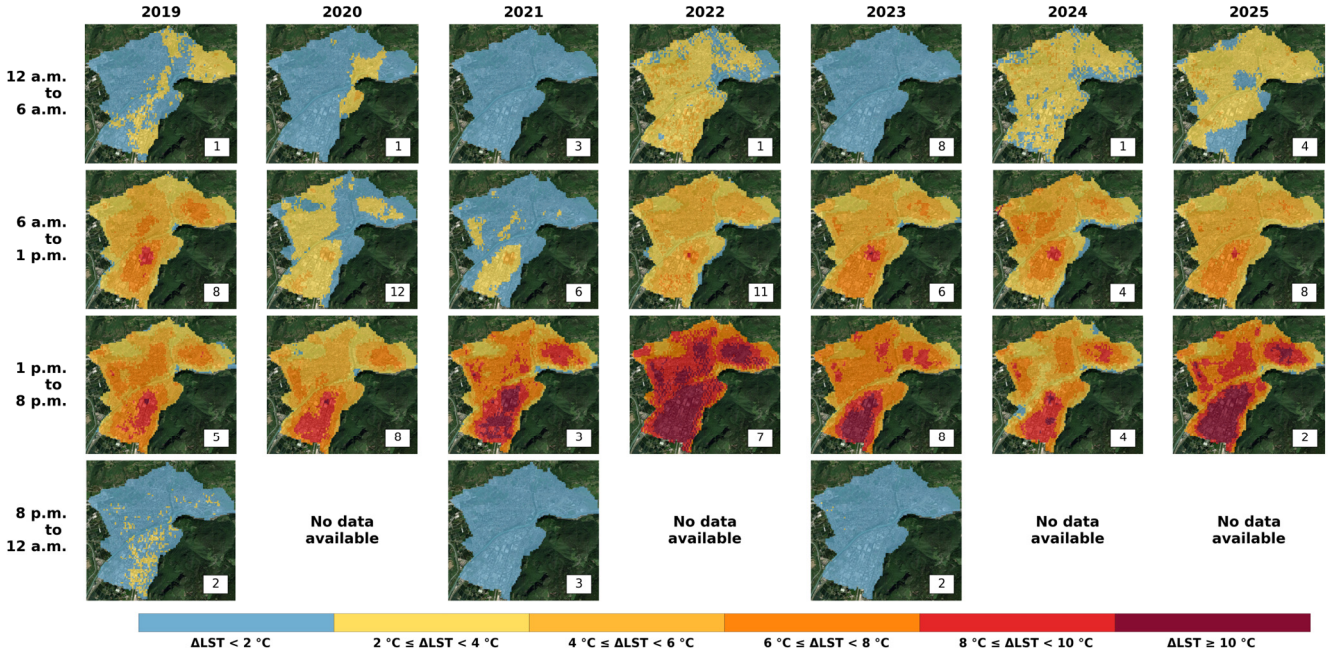

Figure 5. Multi-year spatial analysis of ΔLST ($LST_{urban,pixel} - LST_{rural,mean}$) for Bolzano from 2019 to 2025 at four diurnal periods using ECOSTRESS thermal imagery. The number within each map indicates how many satellite images were used in the ΔLST calculations.

During the nighttime and early morning (12 a.m. to 6 a.m.), the urban area exhibits a very low ΔLST, with a possible indication of an Urban Cooling Island (*UCI*) effect in some areas, especially for 2019–2021 and 2023, and almost the totality of the urban perimeter shows a ΔLST below 2 °C. The difference is more significant for 2022 and 2024, and 2025 has the highest difference for the *LST* records, since most of the urban area shows a *LST* variation between 2 °C and 4 °C, and some hotspots exhibit a ΔLST between 4 °C and 6 °C. The late morning shows an intensification of the *UHI* effect with a ΔLST that consistently increases throughout the years. Even though the industrial zone shows the most critical

variation, with spots displaying a Δ*LST* above 10 °C, the rest of the city also shows a significant increase in *LST*.

The most critical results were observed from 1 p.m. to 8 p.m., representing peak heating within the city and the maximum *UHI* intensity. The highest values are directly tied to the industrial zone of the city. However, it is possible to observe the occurrence of high *UHI* effects within the non-industrial zone, with a Δ*LST* between 6 °C and 10 °C. The results are possible indicators of heatwaves, therefore exhibiting several hotspots and regions above 8 °C in non-industrial areas of Bolzano. The final period of the day, from 8 p.m. to midnight, displays a significant cooling effect, in which most of the territory has a Δ*LST* below 2 °C. The transition represents the beginning of the night cooling effect observed during the first interval of the day. Apart from the spatial analysis of the *LST*, the results also show the temporal gaps present in ECOSTRESS imagery, since no data were available for the last period of the day for 2020, 2022, 2024, and 2025, either because no satellite data were available or the data available were discarded due to low quality.

The association of the building stock within the urban polygon and the Δ*LST* results from satellite images allows a more precise identification of the critical areas and critical buildings, i.e., those more prone to being affected by *UHI* effects based on their location. The results show that industrial buildings show the highest Δ*LST*, while residential buildings usually show the lowest Δ*LST* (Table 2).

Table 2. Summary of Δ*LST* (°C) statistics—mean values and corresponding standard deviations—aggregated by building end-use, year, and period of the day.

Time of Day	Class	2019	2020	2021	2022	2023	2024	2025
12 a.m. to 6 a.m.	Residential	−0.3 (±5.0)	−3.9 (±7.5)	0.0 (±0.6)	2.7 (±0.8)	−3.0 (±1.0)	2.8 (±0.6)	2.8 (±0.9)
	Commercial	1.3 (±3.2)	−3.8 (±6.6)	0.3 (±0.4)	3.1 (±0.9)	−3.0 (±1.1)	2.6 (±0.6)	2.4 (±1.5)
	Industrial	2.0 (±0.4)	−2.1 (±4.5)	0.5 (±0.3)	3.7 (±0.5)	−3.3 (±0.8)	2.6 (±0.5)	2.9 (±1.3)
	Others	−0.4 (±5.2)	−3.7 (±7.6)	−0.0 (±0.7)	2.7 (±0.9)	−2.9 (±1.1)	2.7 (±0.7)	2.6 (±1.2)
6 a.m. to 1 p.m.	Residential	5.0 (±1.1)	2.0 (±0.8)	1.0 (±1.0)	4.6 (±0.9)	5.0 (±0.9)	5.1 (±1.1)	4.9 (±0.9)
	Commercial	5.9 (±1.1)	2.6 (±1.0)	1.7 (±0.9)	5.0 (±0.8)	6.0 (±1.2)	5.5 (±1.3)	5.7 (±0.9)
	Industrial	7.0 (±1.4)	3.6 (±0.6)	2.8 (±0.9)	5.5 (±0.8)	7.1 (±0.9)	6.7 (±1.3)	6.6 (±0.6)
	Others	5.0 (±1.1)	2.0 (±0.9)	1.0 (±0.9)	4.6 (±0.9)	5.0 (±0.9)	4.9 (±1.3)	4.9 (±0.9)
1 p.m. to 8 p.m.	Residential	5.5 (±1.2)	5.0 (±1.1)	7.0 (±1.5)	9.2 (±1.4)	7.1 (±1.2)	6.0 (±1.6)	7.9 (±1.7)
	Commercial	6.7 (±1.3)	6.7 (±1.5)	8.6 (±1.9)	10.5 (±1.4)	8.5 (±1.7)	7.1 (±1.7)	9.7 (±2.2)
	Industrial	7.9 (±1.1)	8.0 (±0.9)	10.3 (±1.7)	11.7 (±1.2)	9.8 (±1.1)	7.7 (±2.1)	11.7 (±1.3)
	Others	5.6 (±1.2)	5.2 (±1.2)	7.1 (±1.5)	9.3 (±1.4)	7.2 (±1.2)	6.2 (±1.5)	8.0 (±1.7)
8 p.m. to 12 a.m.	Residential	1.0 (±0.7)	-	−5.2 (±2.7)	-	−0.2 (±0.9)	-	-
	Commercial	1.4 (±0.7)	-	−2.9 (±3.2)	-	−0.3 (±1.0)	-	-
	Industrial	1.7 (±0.5)	-	0.3 (±0.6)	-	−0.1 (±0.8)	-	-
	Others	1.0 (±0.8)	-	−4.9 (±2.7)	-	−0.3 (±1.0)	-	-

Throughout the years, the first period of the day, 12 a.m. to 6 a.m., showed the lowest *UHI* effects, with three years presenting cooler surfaces than the rural environment, while the other four years showed warmer surfaces. These results can be directly linked with the geographical and topographical aspects of Bolzano, its location within an Alpine basin where three valleys join and the Alpine environmental conditions, and Urban Cooling Island effects (*UCI*). Therefore, factors like insufficient anthropogenic heat to disturb the nocturnal pattern, strong longwave cooling associated with vegetated areas, and cold air pooling can explain the results and especially the low standard deviation across the different classes of buildings.

The second and third periods of the day displayed the most critical changes between the urban and rural environments. These results are directly associated with the built environment, i.e., thermal inertia of impervious elements. Industrial buildings displayed

the highest *UHI* effect, likely related to the combination of less vegetated surroundings, larger impervious surfaces and lower albedo. The effects of the COVID-19 pandemic might have also influenced the years of 2020 and 2021, which presented the lowest deviation, due to the reduction on the anthropogenic heat generation, i.e., reductions in human activity, decline in traffic, and lower industrial emissions. For the remaining years, the results show a pattern for the *LST* variation, with 2022, 2023, and 2025 showing a similar pattern, while 2019 has a higher variation and 2024 presents the highest deviations across all building classes.

The results for the last period of the day, 8 p.m. to 12 a.m., showed a balance between *UHI* and *UCI* effects that can be driven by several meteorological factors such as heatwaves occurrence and intensity, cloud cover, urban canyon ventilation, and synoptic circulation in Alpine regions. This transition period characterizes a complex occurrence within the *UHI/UCI* analysis in mountainous locations. The *UHI* effects at the end of the afternoon and night period within the urban area of Bolzano, with a reduced variation when compared to the diurnal effect but still showing significant variation. Except for 2023, which showed cooler surfaces for most of building classes, all the other years displayed a considerable ΔLST.

Thermal and radiative results show that, despite 2021 not displaying the highest *UHI* effect, a significant difference between the rural and the different urban environments is evident (Table 3). Air temperature clearly shows that the industrial area, represented by *SU2*, has the warmest environment, while the station at the city center (*SU1*) displays a neutral environment when compared to the rural area. In contrast, the city center station exhibited lower temperatures than the station located on the edge of the urban area. This aspect could be explained by the position of the *SU1*, possible benefits from valley-wind ventilation, and the impact of the green infrastructure surrounding the weather station. The third station (*SU3*) displayed a transition profile, being warmer than the rural area (*SR*) but with an intermediate condition compared to the extreme values seen at the industrial zone (*SU2*).

Table 3. Statistical deviations (mean, standard deviation, minimum, and maximum) for thermal and radiative contrasts among four meteorological stations: *SR* (rural), *SU1* (urban core), *SU2* (industrial district), and *SU3* (urban–rural boundary). Pairwise deviations represent hourly temperature and relative humidity and the daily integrated global horizontal radiation. Deviations are calculated as A−B, meaning negative values indicate greater values at station B.

Variable	Metric	*SR-SU1*	*SR-SU2*	*SR-SU3*	*SU1-SU2*	*SU1-SU3*	*SU2-SU3*
Air Temperature (°C)	Mean (Std)	0.2 (±1.5)	−2.3 (±1.4)	−0.9 (±1.2)	−2.5 (±0.7)	−1.1 (±0.9)	1.5 (±0.8)
	Minimum	−5.2	−9.2	−6.2	−5.6	−3.9	−1.1
	Maximum	6.6	4.4	4.5	−0.6	2.4	5.3
Relative Humidity (%)	Mean (Std)	16.1 (±10.9)	16.8 (±9.7)	9.2 (±8.9)	0.7 (±4.2)	−6.9 (±7)	−7.6 (±5.8)
	Minimum	−28.7	−27.6	−27.4	−22.7	−36.8	−30.3
	Maximum	51.7	54.5	49.2	21.9	10.2	8.9
Global Hor. Irradiation (Wh m^{-2} day^{-1})	Mean (Std)	−113.0 (±494.4)	19.3 (±429)	−23.6 (±502.7)	132.3 (±193.6)	89.5 (±207.5)	−42.8 (±212.6)
	Minimum	−1577	−1388	−1747	−316	−512	−564
	Maximum	1879	1736	2015	763	670	665

In contrast, relative humidity results showed that the rural area is the most humid while the industrial zone presented the driest environment. These results clearly displayed the influence of the vegetation and the evaporative cooling for the rural station, while the urban environment of station *SU2* showed the opposite effect, with an amplification of urban heating mostly due to impervious surfaces.

The daily global radiation results showed that the *SU1* has the highest radiation levels, mainly related to less obstruction for the surroundings. The remaining stations displayed

lower radiation, since they are closer to the mountainous environment and the less-exposed topographical context. The results clearly depicted that the industrial area, with the highest *UHI* effect, is dominated by the combination of heat storage, imperviousness, and low moisture over the radiative component. Therefore, the results were coherent with the patterns displayed by the satellite imagery analysis.

3.2. UBEM Analysis

The following analysis discusses the results of the parametric *UBEM* simulation for the months of June, July, and August, performed on 253 residential buildings within the urban boundary of Bolzano (Figure 6). The simulations considered three different envelope configurations, five *WWRs*, and four weather files, resulting in 15,180 EnergyPlus simulations.

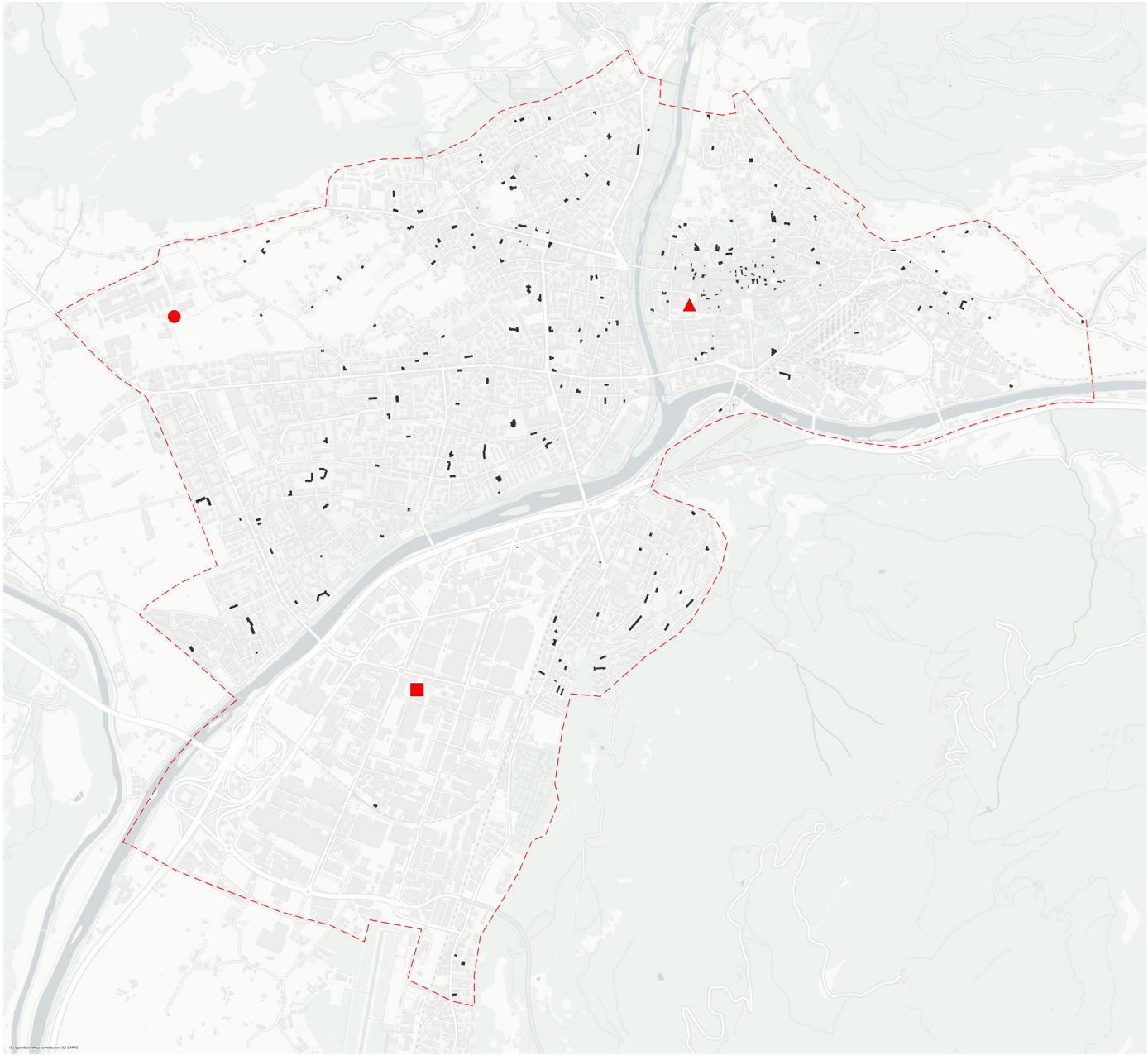

Figure 6. Sample of residential buildings (black) represented within the urban delimitation of Bolzano (red dashed line) and the weather stations *SU1* (red triangle), *SU2* (red square), and *SU3* (red circle).

The selected building sample spans a wide quantitative range of urban and thermal conditions. Median building height is 15.0 m (*IQR*: 9.9–18.0 m), capturing both low-rise and more compact mid-rise configurations, while building footprint area shows substantial variability, with a median of 214 m^2 (*IQR*: 119–347 m^2). This variability is reflected in the enclosed volume, which has a median value of 2713 m^3 (*IQR*: 1364–5303 m^3), indicating that the sample is not dominated by a single building typology but represents a range of sizes and compactness levels across the urban fabric.

Shading conditions further differentiate the buildings. Mean shading angles have a median of 26.9° (*IQR*: 18.3–51.9°), while maximum shading angles reach 47.0° (*IQR*: 36.0–74.0°), highlighting the coexistence of relatively open settings and dense urban environments with strong obstruction and reduced sky exposure. These morphological contrasts are accompanied by clear differences in observed summer surface temperatures, as expressed by the Δ*LST* for 2021 from 1 p.m. to 8 p.m., which shows a median value of 7.3 °C (*IQR*: 6.3–8.1 °C). This confirms that the sample includes buildings exposed to both moderate and pronounced *UHI* conditions, providing a robust basis for interpreting the energy and comfort results presented in this section.

The *EUI* results show, that across all weather stations and envelopes, cooling energy needs increase proportionately to *WWR* (Figure 7). Regarding the building envelope, buildings with no insulation are more affected by the change in the station and the increase in glazed surfaces. Still, on the envelope effect, while the highly insulated envelopes are desirable during cold seasons, the heat trapped inside becomes a factor that significantly increases the *EUI* during summer months, especially in higher *WWR* buildings.

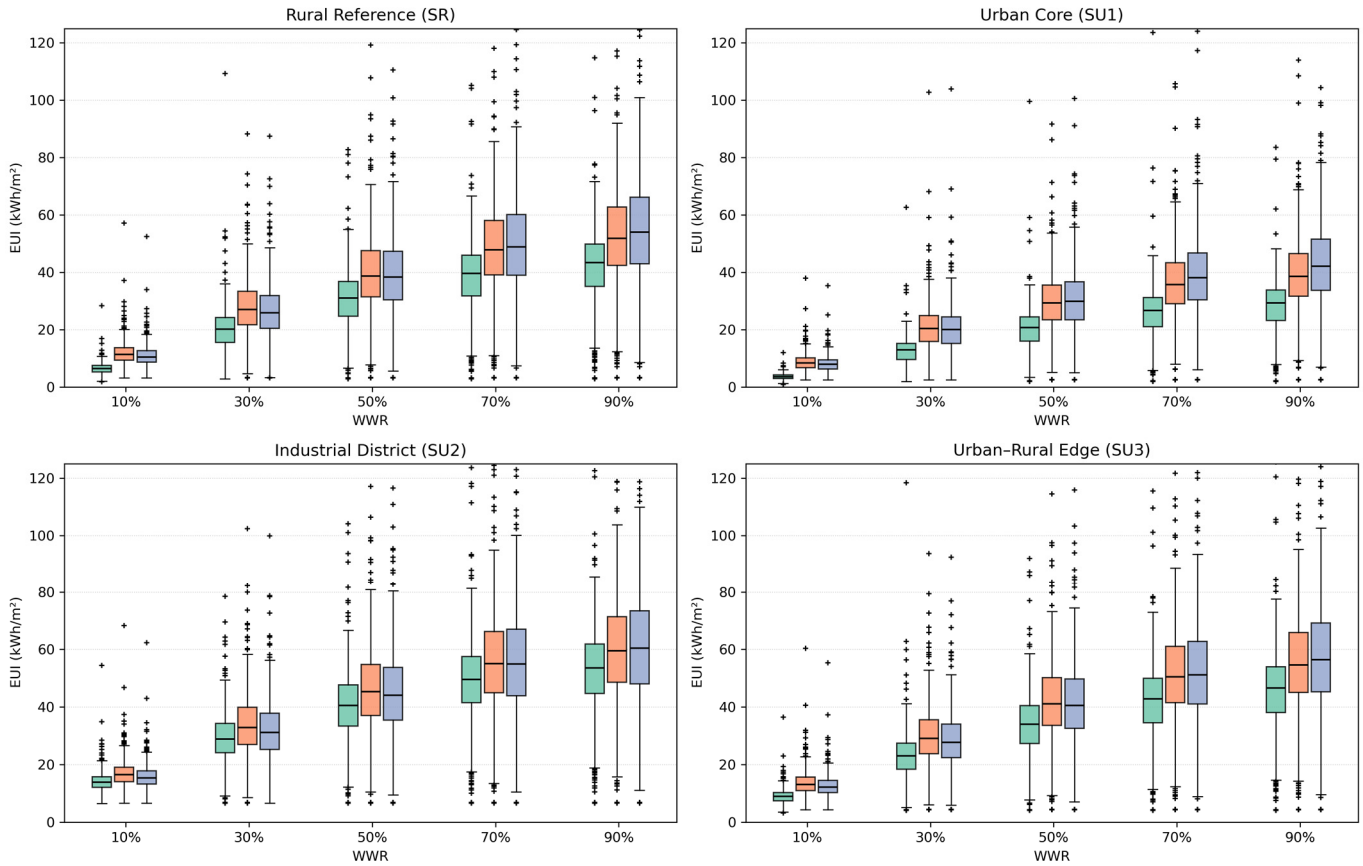

Figure 7. Energy Use Intensity (*EUI*) as a function of window-to-wall ratio (*WWR*) for the four microclimatic stations (*SR*, *SU1*, *SU2*, *SU3*). Envelope types are indicated by color: no insulation (green), well-insulated envelope (orange), and nearly zero building envelope (purple).

The *UHI* pattern observed in satellite imagery does not translate into a simple "urban core equals higher cooling demand" relationship in the simulations, which might also be related to the placement of the weather stations and the morphology of their surroundings. Across all envelopes and *WWRs*, the urban core weather file (*SU1*) consistently produced the lowest period-integrated cooling *EUI*, with a median reduction of ~26% relative to the rural reference (*SR*) (*IQR* ≈ −33% to −23%). In contrast, the industrial district (*SU2*) yields the highest cooling *EUI*, typically ~15–30% above *SR*.

The sub-daily weather comparison supports the explanation of the previous results (Table 4). *SR* is cooler than *SU1* at night (*SR-SU1* ≈ −1.2 °C, meaning *SU1* is warmer), but *SU1* is cooler during the daytime, especially in the afternoon (*SR-SU1* ≈ +1.4 °C), and *SR* remains substantially more humid across all periods (e.g., +26 pp at night). Consistently, the sub-daily energy breakdown shows that the *SR-SU1 EUI* gap is dominated by afternoon and morning cooling, while the nighttime contribution is small (nighttime cooling represents only ~2% of total *EUI* and explains <1% of the *SR-SU1* difference). At the same time, the results confirm that high *WWR* combined with highly insulated envelopes amplifies sensitivity to weather forcing and can increase the risk of overheating under warmer microclimates and future climate conditions.

Table 4. Sub-daily deviations between the rural reference (*SR*) and the urban core (*SU1*). Air temperature and relative humidity are reported as mean (±standard deviation) of hourly differences within each period; cooling energy use intensity (*EUI*) is reported as median (interquartile range, *IQR*) of period-integrated values across all building configurations. Differences are computed as *SR-SU1* (negative values indicate higher values at *SU1*).

Period	ΔTa (°C), Mean (±std)	ΔRH (pp), Mean (±std)	ΔEUI (kWh m^{-2}), Median (IQR)
Night	−1.2 (±1.4)	26.2 (±9.6)	0.07 (0.00–0.16)
Morning	0.5 (±0.5)	14.8 (±3.9)	1.94 (0.47–3.67)
Afternoon	1.4 (±0.6)	8.6 (±4.4)	4.76 (2.25–6.74)
Evening	0.1 (±0.9)	14.7 (±8.1)	1.43 (0.79–2.02)
Total	—	—	8.26 (3.69–12.48)

PMV results follow the same monotonic pattern observed for the *EUI*. Considering the horizontal red dashed lines indicating the thermally neutral conditions (Figure 8), increasing *WWR* leads to a systematic shift of *PMV* toward positive (warm) values and a widening of variability, particularly for well-insulated and nearly zero envelopes and in urban microclimates. Several configurations at high *WWR* exceed the upper comfort threshold, highlighting increased overheating risk under warm urban conditions. The results showed that non-insulated buildings presented a higher variation in *PMV*. While the average values display most of the buildings within the neutral interval (±0.5), the non-insulated buildings with the lowest *WWR* and using the *SU1* weather data display a slight cold discomfort. Additionally, from 50% of glazed surfaces, well-insulated and nearly zero energy building envelopes displayed a slightly warm condition. Despite the small discomfort occurrence, the average values show that they are significantly close to the neutral condition.

Taking the previous results for *EUI* into consideration, a direct correlation can be made between energy needs and *PMV*. The average results showed that, by reducing *EUI*, *PMV* also decreases and the same is valid when increasing energy needs. However, more energy for cooling does not translate into better thermal comfort conditions, but rather into more warm discomfort due to overheating, which is mainly caused by the combination of high *WWR* and the highly insulated envelope. These results show that combining an analysis of energy and thermal comfort is necessary to address the urban scenario, since more efficient

envelopes are not the main determinants of building performance in terms of energy needs and thermal comfort, especially when variables as *WWR* are considered.

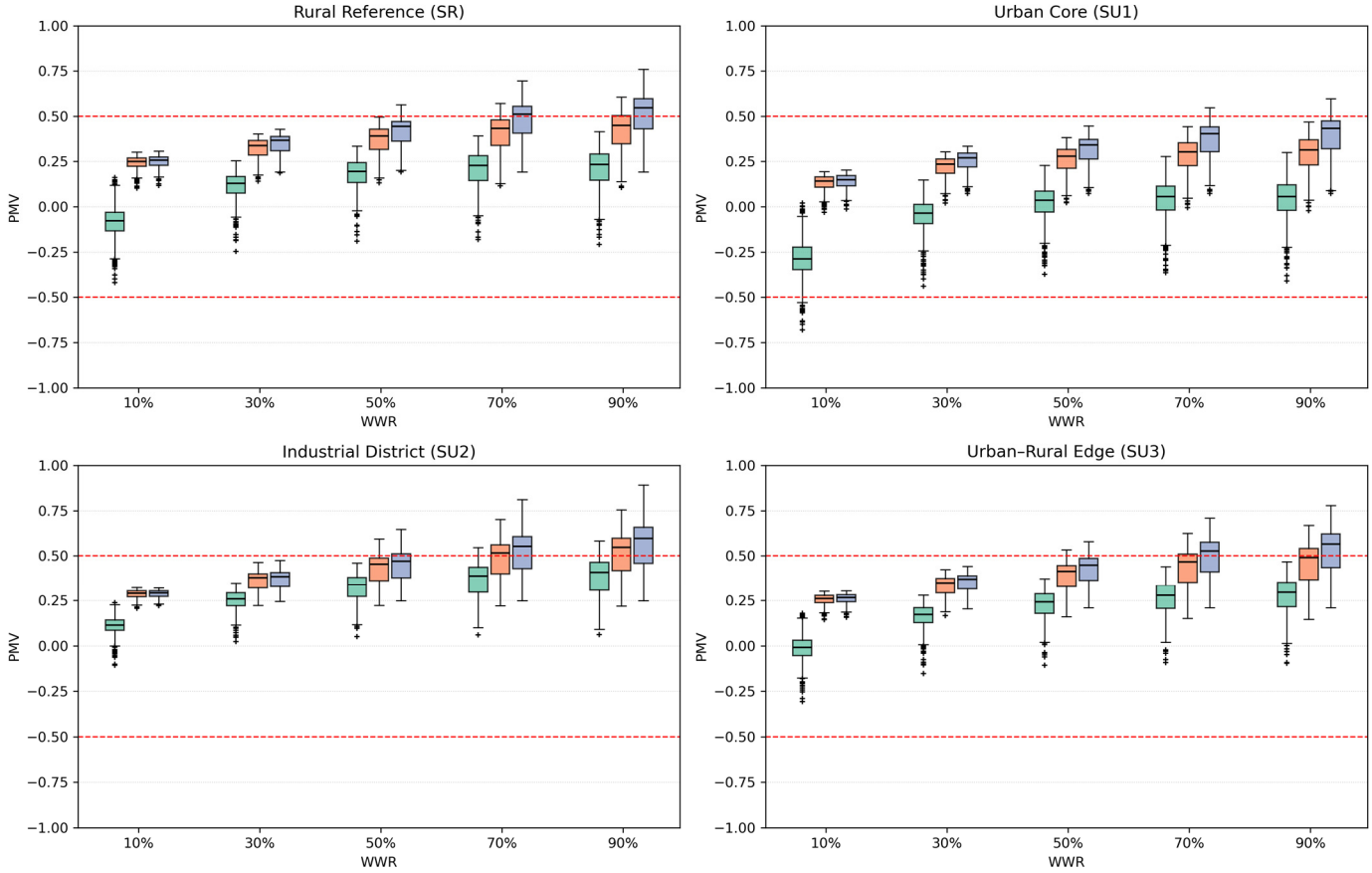

Figure 8. Predicted Mean Vote (*PMV*) as a function of window-to-wall ratio (*WWR*) for the four microclimatic stations (*SR*, *SU1*, *SU2*, *SU3*). Envelope types are indicated by color: no insulation (green), well-insulated envelope (orange), and nearly zero building envelope (purple). The red dashed lines denote the thermal comfort range ($-0.5 \leq PMV \leq +0.5$).

The ANOVA results allowed for the determination of the statistical significance of the different parameters associated with the *UBEM* results, by addressing the statistical effects of the envelope, weather conditions, and the *WWR*. The ANOVA considered envelope type, weather data, and *WWR* as fixed effects, while the repeated simulations and their embedded building geometries were accounted for as random effects within the analysis. Moreover, by applying the mixed-effects ANOVA, we were able to state whether the differences observed in the outputs had a statistical significance across the different simulations performed. Table 5 results show that all three models converged and retained a high explanation capability. The marginal effects showed that, by considering only the three parameters, the models were able to explain more than 50% of the variance and, by considering also the conditional effects from the different simulation, more than 80% of the variance could be explained. While *EUI* offers a significant increase in the capacity to explain variance, by considering conditional effects, the *PMV* model displays a high result already with the marginal effects. These results allowed the researchers to state that the differences highlighted in summer months are robust and not directly related to a random variability within the different models, but rather associated with the envelope, weather data source, and the *WWR*.

Table 5. Summary of mixed-effects ANOVA results and marginal, unique effect sizes (η^2) of fixed factors for *EUI* and *PMV* (*** indicates $p < 0.001$).

Fixed Effect	*EUI*	*PMV*	η^2 (*EUI*)	η^2 (*PMV*)
Envelope	***	***	small	large
Weather Station	***	***	small	medium
WWR	***	***	large	medium
Envelope × *WWR*	***	***	small	medium
Random Effect (Group)	✓	✓	-	-
Marginal R^2	0.58	0.75	-	-
Conditional R^2	0.90	0.88	-	-

Considering not only the statistical significance of the fixed factors, but also their effect sizes, allowed for the ranking of influences and the identification of the variables that most strongly affected the simulation outputs. The results show that different performance indicators are dominated by different factors. For summer cooling energy use intensity (*EUI*), the window-to-wall ratio (*WWR*) exhibits the largest effect size, confirming façade transparency as the primary driver. In contrast, Predicted Mean Vote (*PMV*) is most strongly influenced by building envelope insulation, which shows a large effect size, exceeding that of *WWR*. This highlights the dominant role of envelope thermal properties in shaping indoor thermal sensation, particularly under warm conditions. Across all indicators, weather station (microclimatic conditions) shows a small to medium effect size, indicating a systematic but secondary influence compared to building design variables. The interaction between envelope insulation and *WWR* has a limited effect on *EUI* and a moderate effect on *PMV*, suggesting that non-linear façade–envelope interactions primarily affect thermal comfort rather than summer energy consumption.

Moving beyond the assessment of statistical significance and effect size derived from the ANOVA and η^2 analyses, the evaluation of *RMSE* provides insight into the magnitude of deviations between weather stations, with particular emphasis on the urban context. Hourly *RMSE* was used to assess short-term differences among the urban weather stations (*SU1*, *SU2*, and *SU3*), focusing on their temporal representativeness within the urban area (Figure 9). This analysis isolates instantaneous deviations and complements the previous results based on aggregated indicators by highlighting how urban microclimates diverge at the hourly scale.

For thermal comfort, the magnitude of hourly deviations is not negligible. Median *PMV RMSE* between urban station pairs spans roughly 0.09–0.23, with the smallest deviations observed for *SU2–SU3* and the largest for *SU1–SU2*. This corresponds to a meaningful fraction of the neutral comfort band (±0.5 *PMV*). These results indicate that different urban stations can produce materially different short-term comfort profiles. In contrast, hourly *EUI* deviations are comparatively small and are not interpreted further, since hourly *EUI* mainly reflects short-term fluctuations rather than meaningful differences in long-term energy performance. For this reason, hourly *EUI* deviations are not interpreted further, and energy-related representativeness is instead examined using aggregated temporal metrics.

When the analysis is extended to sub-daily and daily time scales, *RMSE* magnitudes decrease. Daily *PMV RMSE* medians range from about 0.07 (*SU2–SU3*) to about 0.22 (*SU1–SU2*) (Table 6). Sub-daily results show that deviations vary across time-of-day periods, but the relative ranking among station pairs remains stable. Across aggregations, *SU1–SU2* consistently exhibits the largest deviations, *SU1–SU3* is intermediate, and *SU2–SU3* shows the smallest deviations. This persistence indicates that the differences are not driven by random hourly noise but reflect systematic microclimatic contrasts within the urban area.

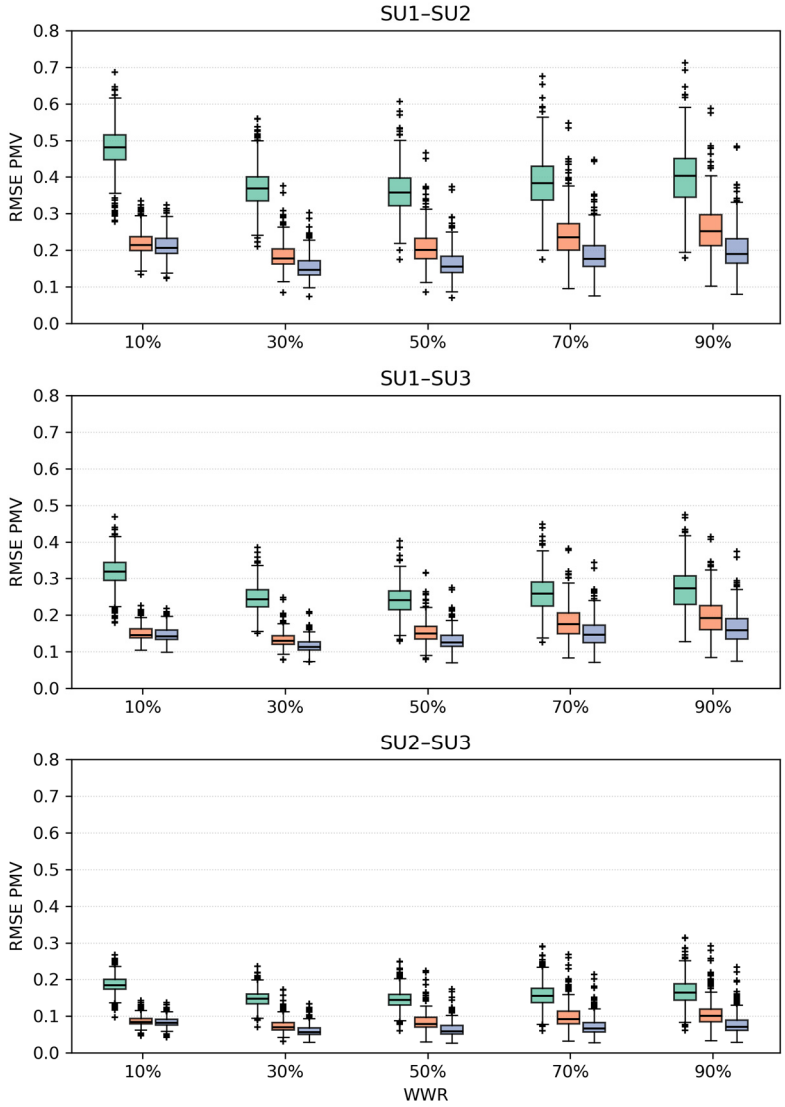

Figure 9. Hourly *RMSE* distributions of *PMV* for pairwise comparisons among urban weather stations (*SU1–SU2*, *SU1–SU3*, *SU2–SU3*). Boxplots are grouped by window-to-wall ratio (*WWR*) and colored by envelope configuration: no insulation (green), well-insulated envelope (orange), and nearly zero building envelope (purple).

Table 6. Summary statistics (median and interquartile range, *IQR*) of hourly, sub-daily, and daily *RMSE* for *PMV* for pairwise comparisons among urban weather stations (*SU1–SU2*, *SU1–SU3*, *SU2–SU3*). Values are aggregated across all building configurations and window-to-wall ratio (*WWR*) levels.

Pair	Hourly PMV	Sub-Daily PMV	Daily PMV
SU1–SU2	0.2 (0.2–0.4)	0.2–0.3	0.2 (0.2–0.3)
SU1–SU3	0.2 (0.1–0.2)	0.1–0.2	0.2 (0.1–0.2)
SU2–SU3	0.1 (0.1–0.1)	0.1–0.1	0.1 (0.0–0.1)

This behavior is consistent with the meteorological differences reported in Table 3, where sustained contrasts in air temperature and relative humidity are observed between urban stations, and where daily integrated global horizontal radiation also shows non-negligible differences. While temporal aggregation dampens short-term variability, these underlying meteorological patterns are preserved and continue to influence thermal comfort outcomes. Overall, the sub-daily and daily *RMSE* results confirm that temporal

aggregation reduces, but does not eliminate, the impact of urban microclimate heterogeneity on comfort metrics, reinforcing the relevance of weather station selection beyond the hourly scale.

The previous analyses showed that urban weather stations differ in their ability to represent thermal comfort conditions, particularly at short time scales, and that these differences are linked to persistent microclimatic contrasts within the urban area. However, these results do not clarify whether such differences can be explained by spatial proximity between buildings and weather stations. To address this point, the analysis is extended by explicitly examining the relationship between building–station distance and *RMSE*. The distance-based analysis evaluates whether buildings located closer to their closest urban weather station exhibit lower *RMSE* values, and therefore better representativeness, compared to more distant buildings. When *RMSE* is compared against building–station distance, the relationship is weak for all outputs (Table 7). Correlation coefficients between distance and *RMSE* to the closest station remain low at both temporal scales. The strongest association is found for *PMV* (Pearson $r = 0.14$ hourly; $r = 0.16$ daily; Spearman $\rho = 0.12$–0.13) and *EUI* is near zero ($r = 0.05$; $\rho = 0.01$–0.02). In practical terms, even the highest correlation explains less than 3% of the variance in *RMSE*.

Table 7. Correlation coefficients (Pearson r and Spearman ρ) between building–station distance and *RMSE* relative to the closest weather station for *EUI* and *PMV* at hourly and daily aggregation levels.

Metric	Aggregation	Pearson r	Spearman ρ
EUI	Hourly	0.05	0.01
	Daily	0.05	0.02
PMV	Hourly	0.14	0.12
	Daily	0.16	0.13

Overall, distance alone is not a reliable predictor of representativeness within the urban area, since the observed associations are consistently weak. While earlier results demonstrated that meteorological differences between stations influence comfort outcomes, the distance analysis suggests that these differences are not spatially smooth or radially organized around the stations. Instead, local urban characteristics and microclimatic patterns appear to dominate over simple geometric proximity.

Importantly, this finding does not contradict the previous *RMSE* results but rather refines their interpretation. Weather station selection matters, particularly for short-term comfort analyses, yet there is no single "preferred" station based solely on distance from a given building. This highlights a key limitation of distance-based approaches for weather file assignment in urban building energy modeling. Moreover, the distance analysis confirms that urban representativeness cannot be inferred from proximity alone, reinforcing the need for weather station selection strategies that account for microclimatic context rather than spatial distance.

Taken together, the results show that the influence of urban weather station selection on *UBEM* outcomes is metric- and scale-dependent. While design-related parameters dominate cooling energy use, thermal comfort indicators are consistently more sensitive to microclimatic differences among urban stations. These differences are most evident at the hourly scale, partially attenuated through sub-daily and daily aggregation, yet remain structured across time scales, reflecting persistent local meteorological contrasts. At the same time, the distance-based analysis shows that spatial proximity explains little of the observed variability, with consistently weak correlations between distance and *RMSE* to the closest station ($|r| \leq 0.16$ and $|\rho| \leq 0.13$). This reconciles the apparent contrast between meteorological relevance and spatial representativeness: weather station choice matters,

but not because of distance; rather, it is because of the underlying urban microclimatic context. Overall, the combined analyses highlight that urban weather representativeness cannot be inferred from a single criterion and must be evaluated jointly across performance metrics, temporal scales, and local climatic characteristics.

4. Method Limitations, Scalability, and Research Outlook

The proposed workflow integrates satellite *LST* with ground meteorological datasets to produce *UHI*-informed boundary conditions for *UBEM*. Its robustness and transferability depend on remote-sensing sampling, the definition of reference conditions, station representativeness, and modeling assumptions that frame the interpretation of the results.

4.1. Limitations and Future Studies

First, ECOSTRESS provides high spatial detail but irregular temporal sampling, which can under-represent specific diurnal phases and reduce comparability across years when overpass times differ. This limitation can be mitigated by extending the observation window across multiple years, combining ECOSTRESS with complementary sensors, and reporting sampling density per diurnal bin to contextualize hotspot persistence.

Second, *LST*-based *UHI* metrics are not always a direct proxy for near-surface air temperature. Surface–air decoupling can be substantial under specific wind, humidity, and cloud regimes; therefore, Δ*LST* should be interpreted as a surface overheating indicator rather than an atmospheric *UHI* measure. Future work should explicitly relate Δ*LST* to air-temperature contrasts using co-located observations (or short campaigns) and assess how meteorological regimes modulate the *LST*–air relationship.

Third, the rural reference definition (buffer size and location) may influence Δ*LST* magnitude, particularly in complex topography where elevation, shading, and valley flows can vary over short distances. This suggests testing alternative rural references (multiple candidates and sensitivity ranges) and adopting objective criteria (e.g., elevation bands and homogeneous land cover) to quantify uncertainty in the reference baseline.

Fourth, station-driven boundary conditions inherit sensor-specific biases and exposure effects that can propagate into energy and comfort outputs. This motivates (i) clearer documentation of sensor sitting and immediate surroundings (supported here through *LCZ* characterization) and (ii) extending the station network, where possible, to better capture intra-urban gradients.

Fifth, the ground-based comparison and *UBEM* simulations are a warm-season proof-of-concept. Because only June–August 2021 was simulated, seasonal variability and winter-time behavior are not addressed, and sensitivities may differ under anomalous summers compared with long-term climatology. Future work should therefore expand the analysis to multi-year and multi-season periods, including explicit heatwave subsets and, where relevant, winter inversion conditions typical of valley environments.

Finally, the *UBEM* used Ideal Loads cooling and standardized internal gains and schedules. These assumptions enable controlled sensitivity testing, but they do not represent operational variability, occupant behavior, adaptive actions, or system constraints. A logical next step is to validate outputs against measured energy use and, when available, indoor temperature observations, and to test more realistic *HVAC* configurations and control strategies.

4.2. Scalability and Transferability

The workflow is scalable because the satellite component can be largely automated (scene screening, masking, diurnal grouping, Δ*LST* mapping), and the *UBEM* component can run parametrically once building archetypes and weather files are defined. Scalability

is nevertheless constrained by (i) the number and quality of ground stations needed to represent intra-urban microclimates, (ii) the effort required to harmonize and quality-control sub-hourly observations into consistent EPW inputs, and (iii) computational cost when extending to large building stocks, multiple years, and multiple climate scenarios.

Transferability across cities should rely on station-selection and weather-assignment strategies grounded in microclimatic context rather than distance alone. In this direction, *LCZ* and morphology-based classification can be extended from station characterization to systematic assignment at the building or neighborhood scale, including mixed-*LCZ* buffers in transition areas. Where stations are sparse, the method can still be applied by using a limited set of representative station datasets to define scenario envelopes (e.g., "industrial-like", "core-like", "edge-like") rather than a single deterministic "urban weather" file.

5. Conclusions

This study addressed a key gap in urban climate–energy workflows: satellite products can resolve intra-urban thermal heterogeneity, but *UBEM* requires hourly atmospheric boundary conditions that are often approximated using a single reference station. We proposed and tested an integrated workflow that combines ECOSTRESS land surface temperature (*LST*) with measured station datasets to (i) map warm-season surface *UHI* patterns and (ii) quantify how station selection affects simulated cooling demand and comfort.

Using Bolzano (Italy, Alpine valley) as a case study, ECOSTRESS scenes (May–August 2019–2025) were processed to derive diurnal Δ*LST* patterns and identify recurrent hotspots. In parallel, one rural and three urban stations (core, industrial, edge) were quality-controlled, harmonized to hourly resolution, and converted into EPW inputs. These station-specific weather files were then used to drive a parametric EnergyPlus *UBEM* campaign for 253 residential buildings with three envelope levels and multiple window-to-wall ratios (*WWR*).

Results show a clear diurnal asymmetry in surface *UHI* intensity, with the strongest urban–rural contrasts occurring from early afternoon to evening and hotspot expansion beyond the industrial zone in some years. Ground measurements confirmed persistent intra-urban differences: during summer 2021, the industrial station (*SU2*) was on average ~2.3 °C warmer than the rural reference and ~2.5 °C warmer than the urban-core station, while urban sites generally exhibited lower relative humidity. In *UBEM* simulations, cooling demand increased systematically with *WWR* across envelopes, and *WWR* explained most of the variance in cooling energy and discomfort probability. Crucially, the choice of measured weather dataset introduced consistent shifts in outcomes: the industrial dataset yielded the highest cooling demand (~15–30% above the rural case), while the urban-core dataset yielded the lowest (~20–35% below the rural case). This demonstrates that "urban climate" is not a single condition even within a compact valley city, and that intra-urban microclimates can alter *UBEM* results at a magnitude comparable to, or larger than, the rural–urban contrast commonly assumed.

Station representativeness could not be inferred from proximity alone. Distance did not show a monotonic relationship with output similarity (*RMSE*), indicating that microclimatic context is a more reliable criterion for weather assignment. Overall, the proposed workflow provides a practical route to incorporate *UHI* heterogeneity into *UBEM* boundary conditions, while the present implementation should be interpreted as a warm-season proof-of-concept due to limited ground-data duration and simplified operational assumptions.

Author Contributions: Conceptualization, M.A.d.S., G.B., A.G. and G.P.; methodology M.A.d.S., G.B. and G.P.; writing—original draft preparation, M.A.d.S. and G.B.; writing—review and editing, M.A.d.S., G.B., A.G. and G.P.; supervision, G.P.; funding acquisition, A.G. and G.P. All authors have read and agreed to the published version of the manuscript.

Funding: This study was carried out within (1) the "Climate Resilient Strategies by Archetype-based Urban Energy Modelling (CRiStAll)" project, funded by the European Union; Next Generation EU within the PRIN 2022 PNRR program (D.D.1409 of 14/09/2022 Ministero dell'Università e della Ricerca); M4C2, I 1.1; and (2) the "Adapting to Climate Change Impact: Crafting South Tyrol's Cooling Future for Energy Resilience (CoolST)" project, funded by the Autonomous Province of Bolzano/Bozen—South Tyrol with funding measure "South Tyrol Climate Plan 2040", year 2024 (resolution of the Provincial Government on 18 July 2023, no 595). Part of this study was developed in the framework of the PhD Research Scholarship "Development of urban building energy models to support the definition of energy policies by municipalities and local public administrations" (DM 118/2023). This manuscript reflects only the authors' views and opinions and the Ministry cannot be considered responsible for them.

Data Availability Statement: The data presented in this study are available on request from the corresponding authors.

Conflicts of Interest: The authors declare no conflicts of interest.

References

1. European Environment Agency. *Trends and Projections in Europe 2024*; European Environment Agency: Copenhagen, Denmark, 2024.
2. Kotlarski, S.; Gobiet, A.; Morin, S.; Olefs, M.; Rajczak, J.; Samacoïts, R. 21st Century Alpine Climate Change. *Clim. Dyn.* **2023**, *60*, 65–86. [CrossRef]
3. Ciancio, V.; Salata, F.; Falasca, S.; Curci, G.; Golasi, I.; de Wilde, P. Energy Demands of Buildings in the Framework of Climate Change: An Investigation across Europe. *Sustain. Cities Soc.* **2020**, *60*, 102213. [CrossRef]
4. Cattivelli, V. Macro-Regional Strategies, Climate Policies and Regional Climatic Governance in the Alps. *Climate* **2023**, *11*, 37. [CrossRef]
5. Stewart, I.D.; Oke, T.R. Local Climate Zones for Urban Temperature Studies. *Bull. Am. Meteorol. Soc.* **2012**, *93*, 1879–1900. [CrossRef]
6. Salvati, A.; Palme, M.; Inostroza, L. Key Parameters for Urban Heat Island Assessment in A Mediterranean Context: A Sensitivity Analysis Using the Urban Weather Generator Model. *IOP Conf. Ser. Mater. Sci. Eng.* **2017**, *245*, 082055. [CrossRef]
7. Sismanidis, P.; Bechtel, B.; Perry, M.; Ghent, D. The Seasonality of Surface Urban Heat Islands across Climates. *Remote Sens.* **2022**, *14*, 2318. [CrossRef]
8. Sadiq Khan, M.; Ullah, S.; Liding, C. Variations in Surface Urban Heat Island and Urban Cool Is-Land Intensity: A Review Across Major Climate Zones. *Chin. Geogr. Sci.* **2023**, *33*, 983–1000. [CrossRef]
9. Hu, L.; Brunsell, N.A. The Impact of Temporal Aggregation of Land Surface Temperature Data for Surface Urban Heat Island (SUHI) Monitoring. *Remote Sens. Environ.* **2013**, *134*, 162–174. [CrossRef]
10. Bokaie, M.; Zarkesh, M.K.; Arasteh, P.D.; Hosseini, A. Assessment of Urban Heat Island Based on the Relationship Between Land Surface Temperature and Land Use/Land Cover in Tehran. *Sustain. Cities Soc.* **2016**, *23*, 94–104. [CrossRef]
11. Karakuş, C.B. The Impact of Land Use/Land Cover (LULC) Changes on Land Surface Temperature in Sivas City Center and Its Surroundings and Assessment of Urban Heat Island. *Asia. Pac. J. Atmos. Sci.* **2019**, *55*, 669–684. [CrossRef]
12. Guo, G.; Wu, Z.; Xiao, R.; Chen, Y.; Liu, X.; Zhang, X. Impacts of Urban Biophysical Composition on Land Surface Temperature in Urban Heat Island Clusters. *Landsc. Urban Plan.* **2015**, *135*, 1–10. [CrossRef]
13. Chang, Y.; Xiao, J.; Li, X.; Weng, Q. Monitoring Diurnal Dynamics of Surface Urban Heat Island for Urban Agglomerations Using ECOSTRESS Land Surface Temperature Observations. *Sustain. Cities Soc.* **2023**, *98*, 104833. [CrossRef]
14. Wang, J.; Cui, X.; Zhao, F.; Huang, M.; Guo, Y.; Wang, Q.; Shao, B.; Tong, Y. ECOSTRESS-Based Analysis of Diurnal Urban Heat Island Intensity and Thermal Dynamics Across LCZ in Six Chinese Cities with Diverse Terrain and Elevation. *IEEE J. Sel. Top. Appl. Earth Obs. Remote Sens.* **2025**, *18*, 15236–15248. [CrossRef]
15. Wei, L.; Sobrino, J.A. Surface Urban Heat Island Analysis Based on Local Climate Zones Using ECOSTRESS and Landsat Data: A Case Study of Valencia City (Spain). *Int. J. Appl. Earth Obs. Geoinf.* **2024**, *130*, 103875. [CrossRef]
16. Pappaccogli, G.; Esposito, A.; Buccolieri, R. Summer Diurnal LST Variability Across Local Climate Zones Using ECOSTRESS Data in Lecce and Milan. *Atmosphere* **2025**, *16*, 377. [CrossRef]
17. Morrison, W.; Grimmond, S.; Kotthaus, S. Simulating Satellite Urban Land Surface Temperatures: Sensitivity to Sensor View Angle and Assumed Landscape Complexity. *Remote Sens. Environ.* **2023**, *293*, 113579. [CrossRef]

18. Xia, W.; Tariq, A.; El-Askary, H.; Aslam, R.W.; Barboza, E.; Kucher, D.E.; Youssef, Y.M.; Kraiem, H. Tackling Data Quality Challenges in Remote Sensing: Solutions for Reliable Urban Heat Island Analysis. *IEEE J. Sel. Top. Appl. Earth Obs. Remote Sens.* **2025**, *18*, 20117–20128. [CrossRef]
19. Vallati, A.; Vollaro, A.D.L.; Golasi, I.; Barchiesi, E.; Caranese, C. On the Impact of Urban Micro Climate on the Energy Consumption of Buildings. *Energy Procedia* **2015**, *82*, 506–511. [CrossRef]
20. Pisello, A.L.; Pignatta, G.; Castaldo, V.L.; Cotana, F. The Impact of Local Microclimate Boundary Conditions on Building Energy Performance. *Sustainability* **2015**, *7*, 9207–9230. [CrossRef]
21. Li, X.; Zhou, Y.; Yu, S.; Jia, G.; Li, H.; Li, W. Urban Heat Island Impacts on Building Energy Consumption: A Review of Approaches and Findings. *Energy* **2019**, *174*, 407–419. [CrossRef]
22. Boccalatte, A.; Fossa, M.; Gaillard, L.; Menezo, C. Microclimate and Urban Morphology Effects on Building Energy Demand in Different European Cities. *Energy Build.* **2020**, *224*, 110129. [CrossRef]
23. Salvalai, G.; Zhu, Y.; Sesana, M.M. From Building Energy Modeling to Urban Building Energy Modeling: A Review of Recent Research Trend and Simulation Tools. *Energy Build.* **2024**, *319*, 114500. [CrossRef]
24. Manapragada, N.V.S.K.; Natanian, J. Urban Microclimate and Energy Modeling: A Review of Integration Approaches. *Sustainability* **2025**, *17*, 3025. [CrossRef]
25. Hong, T.; Chen, Y.; Luo, X.; Luo, N.; Lee, S.H. Ten Questions on Urban Building Energy Modeling. *Build. Environ.* **2020**, *168*, 106508. [CrossRef]
26. He, L.; Geng, X.-W.; Huo, H.-Y.; Lian, Y.; Xi, Q.; Feng, W.; Tu, M.-C.; Leng, P. Simulation of Urban Thermal Environment Based on Urban Weather Generator: Narrative Review. *Urban Sci.* **2025**, *9*, 275. [CrossRef]
27. Ren, Z. A Literature Review on the Use of Weather Data for Building Thermal Simulations. *Energies* **2025**, *18*, 3653. [CrossRef]
28. Salvati, A.; Monti, P.; Coch Roura, H.; Cecere, C. Climatic Performance of Urban Textures: Analysis Tools for a Mediterranean Urban Context. *Energy Build.* **2019**, *185*, 162–179. [CrossRef]
29. Joshi, M.Y.; Rodler, A.; Musy, M.; Guernouti, S.; Cools, M.; Teller, J. Identifying Urban Morphological Archetypes for Microclimate Studies Using a Clustering Approach. *Build. Environ.* **2022**, *224*, 109574. [CrossRef]
30. Esposito, A.; Pappaccogli, G.; Donateo, A.; Salizzoni, P.; Maffeis, G.; Semeraro, T.; Santiago, J.L.; Buccolieri, R. Urban Morphology and Surface Urban Heat Island Relationship During Heat Waves: A Study of Milan and Lecce (Italy). *Remote Sens.* **2024**, *16*, 4496. [CrossRef]
31. Statistical Office of the European Union (Eurostat). *Energy Statistics—Cooling and Heating Degree Days*; Statistical Office of the European Union (Eurostat): Luxembourg, 2021.
32. Istituto Superiore per la Protezione e la Ricerca Ambientale (ISPRA)—Sezione Climatologia Operativa. *Valori Climatici Normali in Italia*; Istituto Superiore per la Protezione e la Ricerca Ambientale (ISPRA)—Sezione Climatologia Operativa: Rome, Italy, 2022.
33. Hook, S.; Hulley, G. *ECOSTRESS Swath Land Surface Temperature and Emissivity Instantaneous L2 Global 70 m V002 [Data Set]*; NASA Land Processes Distributed Active Archive Center: Sioux Falls, SD, USA, 2022. [CrossRef]
34. Mazzarino, P.R.; Finocchiaro, S.; Barbierato, L.; Schiera, D.S.; Bottaccioli, L.; Patti, E. An Automated Tool for Urban Building Energy Modelling: From Sparse Datasets to CityJSON. In Proceedings of the 2024 IEEE International Conference on Environment and Electrical Engineering and 2024 IEEE Industrial and Commercial Power Systems Europe (EEEIC/I&CPS Europe), Rome, Italy, 17–20 June 2024; pp. 1–7.
35. Morales, R.D.; Audenaert, A.; Verbeke, S. Integrating CityJSON with Building Performance Simulation: A Case Study of Summer Indoor Overheating in Antwerp. In Proceedings of the 19th International Building Performance Simulation Association Conference, Brisbane, Australia, 24–27 August 2025.
36. Provincia Autonoma di Bolzano Alto Adige MapView. Available online: https://mapview.civis.bz.it/ (accessed on 22 December 2025).
37. Demuzere, M.; Kittner, J.; Martilli, A.; Mills, G.; Moede, C.; Stewart, I.D.; van Vliet, J.; Bechtel, B. A Global Map of Local Climate Zones to Support Earth System Modelling and Urban-Scale Environmental Science. *Earth Syst. Sci. Data* **2022**, *14*, 3835–3873. [CrossRef]
38. *ANSI/ASHRAE 140-2007*; Method of Test for Evaluating Building Performance Simulation Software. American Society of Heating, Refrigerating and Air-Conditioning Engineers, Inc.: Peachtree Corners, GA, USA, 2007.
39. *EN 16798-1:2019*; Energy Performance of Buildings—Ventilation for Buildings—Part 1: Indoor Environmental Input Parameters for Design and Assessment of Energy Performance of Buildings Addressing Indoor Air Quality, Thermal Environment, Lighting and Acoustics—Modules M1-6. European Committee for Standardization. European Committee for Standardization: Brussels, Belgium, 2019.
40. *EN 15193-1:2021*; Energy Performance of Buildings—Energy Requirements for Lighting—Part 1: Specifications—Module 9. European Committee for Standardization: Brussels, Belgium, 2021.
41. *DPP Nr. 6 Del 18.03.2025*; Regolamento Di Esecuzione in Materia Di Prestazione Energetica Nell'edilizia, in Attuazione Della Direttiva (UE) 2024/1275, e Di Bonus Energia. Provincia Autonoma di Bolzano Alto Adige: Bolzano, Italy, 2025.

42. *ISO 7730:2025*; Ergonomics of the Thermal Environment—Analytical Determination and Interpretation of Thermal Comfort Using Calculation of the PMV and PPD Indices and Local Thermal Comfort Criteria. International Organization for Standardization: Geneva, Switzerland, 2025.
43. Nakagawa, S.; Schielzeth, H. A General and Simple Method for Obtaining R2 from Generalized Linear Mixed-Effects Models. *Methods Ecol. Evol.* **2013**, *4*, 133–142. [CrossRef]
44. Richardson, J.T.E. Eta Squared and Partial Eta Squared as Measures of Effect Size in Educational Research. *Educ. Res. Rev.* **2011**, *6*, 135–147. [CrossRef]

Disclaimer/Publisher's Note: The statements, opinions and data contained in all publications are solely those of the individual author(s) and contributor(s) and not of MDPI and/or the editor(s). MDPI and/or the editor(s) disclaim responsibility for any injury to people or property resulting from any ideas, methods, instructions or products referred to in the content.